WAMS-Based Model-Free Wide-Area Damping Control by Voltage Source Converters

Jinpeng Guo, *Student Member, IEEE,* Ilias Zenelis, *Student Member, IEEE,* Xiaozhe Wang, *Member, IEEE,*
Boon-Teck Ooi, *Life Fellow, IEEE*

Abstract—In this paper, a novel model-free wide-area damping control (WADC) method is proposed, which can achieve full decoupling of modes and damp multiple critical inter-area oscillations simultaneously using grid-connected voltage source converters (VSCs). The proposed method is purely measurement-based and requires no knowledge of the network topology and the dynamic model parameters. Hence, the designed controller using VSCs can update the control signals online as the system operating condition varies. Numerical studies in the modified IEEE 68-bus system with grid-connected VSCs show that the proposed method can estimate the system dynamic model accurately and can damp inter-area oscillations effectively under different working conditions and network topologies.

Index Terms—phasor measurement units, voltage source converters, wide-area damping control, wide-area measurement system

I. INTRODUCTION

POWER system oscillations have been traditionally damped by employing the power system stabilizer (PSS) [1] and Flexible AC Transmission System (FACTS) with Power Oscillation Damping (POD) controller [2]. However, PSS might be ineffective in damping multiple inter-area oscillations [3], while the damping performance of both PSS and FACTS-POD controller may vary with their locations [2]. More recently, growing renewable energy sources (RES) are integrated into the power grids. The inverter-based RES generators may interact with the damping torque, resulting in either improved or deteriorated system stability depending on different working conditions [4], [5]. Meanwhile, considering the flexible controls of inverter-based generations, many efforts have been made to develop effective POD controllers by exploiting the inverter-based generations [6]–[8]. Particularly, voltage source converters (VSCs), serving as the interface between RES and the AC power system, are regarded as new and promising candidates to improve AC system dynamic performance. Compared to the conventional FACTS devices that can control only reactive power, VSCs connected with RES can control both active and reactive power independently, which provides more flexibility in control design [9]. Note that

several FACTS devices equipped with energy storage systems can also control active power, but they share similar features in topology and functions with VSC integrating RES [10]. Therefore, we mainly focus on VSCs for POD in this paper, whereas it is believed that other FACTS devices similar to VSCs can be exploited in the same fashion.

Many control methods have been proposed to enhance the system POD performance using VSCs such as modal linear quadratic Gaussian (LQG) control [3], the traditional PSS-based control [11], mixed H_2/H_∞ output feedback control [12], Lyapunov control theory [8] and sliding mode robust control [6]. Although the robust control methods (e.g., mixed H_2/H_∞ feedback control) provide the designed controllers with some robustness to the uncertainties of parameters and noise, all the aforementioned methods require accurate knowledge of network topology and system parameters when the controllers are designed offline. However, the network may suffer from undetected topology changes and the system parameters may vary in different operation conditions. Therefore, effectiveness of the controllers designed offline may be deteriorated. Such problems are aggravated after the integration of RES. To address these issues, wide-area measurement system (WAMS)-based wide-area damping control (WADC) methods have been proposed in [13], [14]. However, the method proposed in [13] is not purely model-free, requiring the damping coefficients. Also, the method may not be directly implemented by VSCs. Besides, the method proposed in [14] may not optimize the damping performance of multiple modes simultaneously. Several online WADC methods have been discussed in [15], which nevertheless also points out the gap between the online identification and control, as the reduced-order model obtained from the system identification methods may not be the physical model and cannot be related to the real system state variables, making the control design challenging.

In this paper, we propose a novel model-free WADC method using VSCs, which can achieve full decoupling of modes such that the damping performance of multiple inter-area modes can be optimized simultaneously as the system steady-state operating condition varies. Specifically, we first integrate the model of VSCs into the dynamic AC power system model in the form of state-space representation. Next, a perturbation approach is designed to estimate the state matrix A and the input matrix B only from PMU data by exploiting the regression theorem of multivariate Ornstein-Uhlenbeck process [16]. It should be noted that, unlike other measurement-based mode identification methods (e.g., system identification methods),

the estimated A and B correspond to the linearization of the *physical model*, which possesses clear physical interpretations and can be directly utilized in control design. Therefore, the modal linear quadratic regulator (MLQR)-based control method is applied to the estimated A and B to design a wide-area damping controller using VSCs.

To our best knowledge, the proposed method seems to be *the first* model-free WADC strategy that can achieve full decoupling of modes and can target all critical modes simultaneously in various operation conditions and network topologies. The contributions of the paper are summarized below:

- An entirely model-free method is designed to estimate the system state matrix A and the input matrix B in the state-space representation of the *true physical* model of a power system with VSCs. Compared to [17], additional model formulation and mathematical manipulation are conducted for the integration of VSCs. A perturbation approach is also designed to separate A and B from the closed-loop system state matrix.
- Based on the estimated matrices, a MLQR-based WADC method, requiring no knowledge of network model, is proposed to update the control signals of VSCs so that multiple critical inter-area modes can be damped simultaneously without affecting others as the system operating condition varies, as opposed to the model-based WADC methods [3], [6], [8], [11], [12].

The rest of the paper is organized as follows. Section II presents the state-space representation of the AC system with grid-connected VSCs. Section III describes the WAMS-based estimation strategy for the system state matrix A and the input matrix B in the state-space representation. Section IV shows the MLQR-based WADC based on the estimated matrices using VSCs. Section V validates the proposed estimation and control strategy through comprehensive numerical studies. Section VI summarizes the conclusions.

II. System Modeling

A. The Stochastic Model of AC power system

In this paper, we consider the small-signal electromechanical stability around the steady state, in which the rotor angle dynamics dominate. Therefore, the classical generator dynamic model is considered:

$$\dot{\boldsymbol{\delta}} = \omega_0 (\boldsymbol{\omega} - \mathbf{1})$$
$$M \dot{\boldsymbol{\omega}} = \boldsymbol{P_M} - \boldsymbol{P_E} - D (\boldsymbol{\omega} - \mathbf{1}) \tag{1}$$

with

$$P_{ei} = \sum_{j=1}^{N_g} E_i E_j \left(G_{ij} \cos (\delta_i - \delta_j) + B_{ij} \sin (\delta_i - \delta_j) \right)$$

where $\boldsymbol{\delta} = \begin{bmatrix} \delta_1, \delta_2, ..., \delta_{N_g} \end{bmatrix}^T$ is the vector of generator rotor angles, $\boldsymbol{\omega} = \begin{bmatrix} \omega_1, \omega_2, ..., \omega_{N_g} \end{bmatrix}^T$ is the vector of generator rotor speeds and ω_0 is the base value, $M = diag \left(\begin{bmatrix} M_1, M_2, ..., M_{N_g} \end{bmatrix} \right)$ is the inertia coefficient matrix, $D = diag \left(\begin{bmatrix} D_1, D_2, ..., D_{N_g} \end{bmatrix} \right)$ is the damping coefficient matrix, $\boldsymbol{P_M} = \begin{bmatrix} P_{m1}, P_{m2}, ..., P_{mN_g} \end{bmatrix}^T$ is the vector of generators' mechanical power input, $\boldsymbol{P_E} = \begin{bmatrix} P_{e1}, P_{e2}, ..., P_{eN_g} \end{bmatrix}^T$

is the vector of generators' electromagnetic power output, E_i is the constant voltage behind the transient reactance of the ith generator, $G_{ij} + jB_{ij}$ is the (i, j)th entry of the reduced system admittance matrix with only generator buses, and N_g is the number of generators.

Similar to [18], [19], we make a common assumption that load active powers are perturbed by independent Gaussian noise from their base loadings. As previously shown in [19], the load variations can be described by random perturbations at the diagonal elements of the reduced admittance matrix $Y(i, i) = Y_{ii} (1 + \sigma_i \xi_i) \angle \phi_{ii}$, where i is the generator number, ξ_i is a standard Gaussian variable and $\sigma_i{}^2$ describes the intensity of the fluctuations. Hence, the power system dynamic model considering the stochasticity of loads can be described by [20]:

$$\dot{\boldsymbol{\delta}} = \omega_0 (\boldsymbol{\omega} - \mathbf{1})$$
$$M \dot{\boldsymbol{\omega}} = \boldsymbol{P_M} - \boldsymbol{P_E} - D (\boldsymbol{\omega} - \mathbf{1}) - E^2 G \Sigma \boldsymbol{\xi} \tag{2}$$

where $E = diag \left(\begin{bmatrix} E_1, E_2, ..., E_{N_g} \end{bmatrix} \right)$, $G = diag \left(\begin{bmatrix} G_{11}, G_{22}, ..., G_{N_g N_g} \end{bmatrix} \right)$, $\Sigma = diag \left(\begin{bmatrix} \sigma_1, \sigma_2, ..., \sigma_{N_g} \end{bmatrix} \right)$ and $\boldsymbol{\xi} = \begin{bmatrix} \xi_1, \xi_2, ..., \xi_{N_g} \end{bmatrix}^T$. Linearizing (2) around the steady-state operating point gives

$$\Delta \dot{\boldsymbol{\delta}} = \omega_0 \Delta \boldsymbol{\omega}$$
$$M \Delta \dot{\boldsymbol{\omega}} = -\Delta \boldsymbol{P_E} - D \Delta \boldsymbol{\omega} - E^2 G \Sigma \boldsymbol{\xi} \tag{3}$$

which can be further represented in the compact form by substituting $\Delta \boldsymbol{P_E} = \frac{\partial \boldsymbol{P_E}}{\partial \boldsymbol{\delta}} \Delta \boldsymbol{\delta}$:

$$\dot{\boldsymbol{x}} = A_o \boldsymbol{x} + S \boldsymbol{\xi} \tag{4}$$

where $\boldsymbol{x} = [\Delta \boldsymbol{\delta}, \Delta \boldsymbol{\omega}]^T$, $S = \begin{bmatrix} 0, -M^{-1} E^2 G \Sigma \end{bmatrix}^T$, $A_o = \begin{bmatrix} 0 & \omega_0 I_{N_g} \\ -M^{-1} \frac{\partial \boldsymbol{P_E}}{\partial \boldsymbol{\delta}} & -M^{-1} D \end{bmatrix}$ is the open-loop system state matrix, and I_{N_g} is an identity matrix of size N_g. Particularly, $\boldsymbol{x}$ is a vector Ornstein-Uhlenbeck process, which is Gaussian and Markovian.

A_o carries significant information about the system dynamics and stability. For instance, the small-signal stability analysis of a power system is based on analyzing the eigenvalues and eigenvectors of A_o. Conventionally, A_o can be easily calculated if it is assumed that the system dynamic model and the network topology are known, and the system states from the state estimator are accurate. Nevertheless, such assumption may not be true in practice due to network topology errors, bad data, etc. Therefore, an online data-driven method was proposed in [17] to estimate the matrix A_o, which has been shown to be accurate, robust to measurement noise, and adaptive to topology change. However, the formulation in [17] does not consider the presence of VSCs, which in turn is essential considering an increasing number of VSCs due to the growing penetration of RES. The integration of VSCs, on the other hand, makes the matrix estimation challenging, as the impacts of VSCs has to be carefully expressed in the formulation of (4). An approach to separate the open-loop system state matrix A and the input matrix B that quantifies the impacts of VSCs is also needed for the sake of control design. Details will be discussed in Section III.

Lastly, although the 2nd-order generator model is assumed in the proposed methodology, higher-order generator models

with detailed control are used in the simulation study to show the feasibility of the proposed method in practice.

B. VSC model

Since we are interested in the electromechanical stability around the steady state, the VSCs are modelled as power sinks and sources, similar to the approach adopted in [8], which is based on the approximation that fast dynamics of VSCs are much faster than electromechanical dynamics such that VSCs respond instantaneously fast to the power reference change [21].

In order to provide damping support from VSCs, supplementary active and reactive power signals should be added to the steady state references [11]. Hence, the power injections from the buses where VSCs are connected are

$$
\begin{aligned}
\boldsymbol{P_v} &= \boldsymbol{P_{vs}} + \boldsymbol{P_{vd}} \\
\boldsymbol{Q_v} &= \boldsymbol{Q_{vs}} + \boldsymbol{Q_{vd}}
\end{aligned}
\tag{5}
$$

where $\boldsymbol{P_v} = [P_{v1}, P_{v2}, \cdots, P_{vN_v}]^T$ represents the real-time active power references of the VSC; $\boldsymbol{P_{vs}} = \left[P_{vs_1}, P_{vs_2} \cdots P_{vs_{N_v}}\right]^T$ denotes the steady-state active power references; $\boldsymbol{P_{vd}} = \left[P_{vd_1}, P_{vd_2} \cdots P_{vd_{N_v}}\right]^T$ are the references for the supplementary active power generated by the damping controller. The reactive powers $\boldsymbol{Q_v}$, $\boldsymbol{Q_{vs}}$ and $\boldsymbol{Q_{vd}}$ are defined in a similar way. It should be noted that the intermittency of RES is not considered in this paper similar to [22], [23], because the time scale of RES intermittency (a few minutes [24]) is much larger than that of electromechanical dynamics (0.5s-5s [25]). In addition, [8] shows that the fluctuation of the output power of RES may be quickly smoothed out through proper power control (e.g., pitch angle control for wind turbines).

In order to provide damping, the frequency variations of generators are typically used as the feedback signals [8] and we have

$$
\begin{aligned}
\boldsymbol{P_{vd}} &= K_1 \left(\boldsymbol{\omega} - \boldsymbol{1}\right) \\
\boldsymbol{Q_{vd}} &= K_2 \left(\boldsymbol{\omega} - \boldsymbol{1}\right)
\end{aligned}
\tag{6}
$$

where K_1 and K_2 are damping coefficients of the active and reactive power control of VSCs, respectively.

Linearizing (5) and (6) around the steady state gives

$$
\begin{aligned}
\Delta \boldsymbol{P_v} &= \Delta \boldsymbol{P_{vd}} = K_1 \Delta \boldsymbol{\omega} \\
\Delta \boldsymbol{Q_v} &= \Delta \boldsymbol{Q_{vd}} = K_2 \Delta \boldsymbol{\omega}
\end{aligned}
\tag{7}
$$

C. Integration of VSCs into AC system

By applying Kron reduction [26], we can eliminate all buses except the N_g generator buses and the N_v VSC buses as shown in Fig. 1. The active power injection from the bus where the ith generator is connected can be calculated by

$$
\begin{aligned}
P_{ei} = &\sum_{j=1}^{N_g} E_i E_j \left(G_{GGij} \cos \left(\delta_i - \delta_j\right) + B_{GGij} \sin \left(\delta_i - \delta_j\right)\right) \\
&+ \sum_{j=1}^{N_v} E_i V_j \left(G_{GVij} \cos \left(\delta_i - \theta_j\right) + B_{GVij} \sin \left(\delta_i - \theta_j\right)\right)
\end{aligned}
\tag{8}
$$

where V_j and θ_j are the voltage magnitude and voltage angle of VSC bus j. G_{GGij} and B_{GGij} are the equivalent conductance and susceptance between generator buses i and j. G_{GVij} and B_{GVij} are the equivalent conductance and susceptance between generator bus i and VSC bus j.

Similarly, the active and reactive power injections from the bus where the ith VSC is connected can be expressed by

$$
\begin{aligned}
P_{vi} = &\sum_{j=1}^{N_g} V_i E_j \left(G_{VGij} \cos \left(\theta_i - \delta_j\right) + B_{VGij} \sin \left(\theta_i - \delta_j\right)\right) \\
&+ \sum_{j=1}^{N_v} V_i V_j \left(G_{VVij} \cos \left(\theta_i - \theta_j\right) + B_{VVij} \sin \left(\theta_i - \theta_j\right)\right) \\
Q_{vi} = &\sum_{j=1}^{N_g} V_i E_j \left(G_{VGij} \sin \left(\theta_i - \delta_j\right) - B_{VGij} \cos \left(\theta_i - \delta_j\right)\right) \\
&+ \sum_{j=1}^{N_v} V_i V_j \left(G_{VVij} \sin \left(\theta_i - \theta_j\right) - B_{VVij} \cos \left(\theta_i - \theta_j\right)\right)
\end{aligned}
\tag{9}
$$

where G_{VGij} and B_{VGij} are the equivalent conductance and susceptance between VSC bus i and generator bus j. G_{VVij} and B_{VVij} are the equivalent conductance and susceptance between VSC bus i and VSC bus j.

Linearizing the power injections of generators and VSCs (8)-(9) around the steady state yields

$$
\begin{bmatrix}
\Delta \boldsymbol{P_E} \\
\Delta \boldsymbol{P_v} \\
\Delta \boldsymbol{Q_v}
\end{bmatrix}
=
\begin{bmatrix}
\frac{\partial \boldsymbol{P_E}}{\partial \boldsymbol{\delta}} & \frac{\partial \boldsymbol{P_E}}{\partial \boldsymbol{\theta}} & \frac{\partial \boldsymbol{P_E}}{\partial \boldsymbol{V}} \\
\frac{\partial \boldsymbol{P_v}}{\partial \boldsymbol{\delta}} & \frac{\partial \boldsymbol{P_v}}{\partial \boldsymbol{\theta}} & \frac{\partial \boldsymbol{P_v}}{\partial \boldsymbol{V}} \\
\frac{\partial \boldsymbol{Q_v}}{\partial \boldsymbol{\delta}} & \frac{\partial \boldsymbol{Q_v}}{\partial \boldsymbol{\theta}} & \frac{\partial \boldsymbol{Q_v}}{\partial \boldsymbol{V}}
\end{bmatrix}
\begin{bmatrix}
\Delta \boldsymbol{\delta} \\
\Delta \boldsymbol{\theta} \\
\Delta \boldsymbol{V}
\end{bmatrix}
\tag{10}
$$

Since the system is assumed to be in the normal operating state such that the Jacobian matrix is well-conditioned [27], we can represent $\Delta \boldsymbol{P_E}$ by $\Delta \boldsymbol{\delta}$, $\Delta \boldsymbol{P_v}$ and $\Delta \boldsymbol{Q_v}$:

$$
\Delta \boldsymbol{P_E} = A_1 \Delta \boldsymbol{\delta} + A_2 \Delta \boldsymbol{P_v} + A_3 \Delta \boldsymbol{Q_v}
\tag{11}
$$

The detailed expression of A_1, A_2 and A_3 can be found in Appendix A. Substituting the expression of $\Delta \boldsymbol{P_E}$ from (11) to (3) leads to

$$
\begin{aligned}
\begin{bmatrix}
\Delta \dot{\boldsymbol{\delta}} \\
\Delta \dot{\boldsymbol{\omega}}
\end{bmatrix}
&=
\begin{bmatrix}
0 & \omega_0 I_{N_g} \\
-M^{-1} A_1 & -M^{-1} D
\end{bmatrix}
\begin{bmatrix}
\Delta \boldsymbol{\delta} \\
\Delta \boldsymbol{\omega}
\end{bmatrix} \\
&+
\begin{bmatrix}
0 & 0 \\
-M^{-1} A_2 & -M^{-1} A_3
\end{bmatrix}
\begin{bmatrix}
\Delta \boldsymbol{P_v} \\
\Delta \boldsymbol{Q_v}
\end{bmatrix} \\
&+
\begin{bmatrix}
0 \\
-M^{-1} E^2 G \Sigma
\end{bmatrix}
\boldsymbol{\xi}
\end{aligned}
\tag{12}
$$

It can be further represented in the compact form:

$$
\dot{\boldsymbol{x}} = A \boldsymbol{x} + B \boldsymbol{u} + S \boldsymbol{\xi}
\tag{13}
$$

where $\boldsymbol{u} = [\Delta \boldsymbol{P_v}, \Delta \boldsymbol{Q_v}]^T$, $A = \begin{bmatrix} 0 & \omega_0 I_{N_g} \\ \bar{A}_1 & -M^{-1}D \end{bmatrix}$, $B = \begin{bmatrix} 0 & 0 \\ \bar{A}_2 & \bar{A}_3 \end{bmatrix}$. Particularly, $\bar{A}_1 = -M^{-1}A_1$, $\bar{A}_2 = -M^{-1}A_2$ and $\bar{A}_3 = -M^{-1}A_3$.

In order to design the damping controller, the accurate information of A and B in (13) needs to be known. Substituting (7) into (13), B can be embedded in the system state matrix as follows:

$$
\dot{\boldsymbol{x}} = A_c \boldsymbol{x} + S \boldsymbol{\xi}
\tag{14}
$$

where $A_c = \begin{bmatrix} 0 & \omega_0 I_{N_g} \\ \bar{A}_1 & \bar{A}_2 K_1 + \bar{A}_3 K_2 - M^{-1}D \end{bmatrix}$.

Compared with the open-loop matrix A_o in (4) without VSC, the closed-loop system state matrix A_c includes the
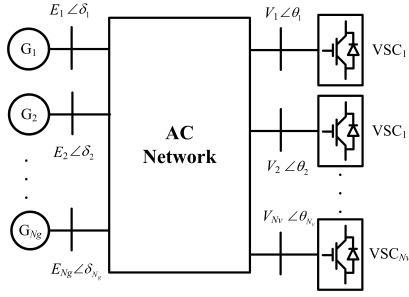
Fig. 1. An AC system integrated with VSCs.

impact of VSCs, as reflected by the new elements $\bar{A}_2 K_1$ and $\bar{A}_3 K_2$. Since the work in [3], [11] has shown that the impact of reactive power on damping control is much smaller than that of active power, the reactive power control for damping is not considered in the rest of paper, i.e., $\Delta \boldsymbol{Q_v}$ is zero by setting K_2 to be zero matrix. As a result, A remains the same as in (13):

$$A = \left[\begin{array}{cc} 0 & \omega_0 I_{N_g} \\ \bar{A}_1 & -M^{-1}D \end{array} \right] \tag{15}$$

B becomes:

$$B = \left[\begin{array}{c} 0 \\ \bar{A}_2 \end{array} \right] \tag{16}$$

A_c becomes:

$$A_c = \left[\begin{array}{cc} 0 & \omega_0 I_{N_g} \\ \bar{A}_1 & \bar{A}_2 K_1 - M^{-1}D \end{array} \right] \tag{17}$$

III. THE PROPOSED WAMS-BASED METHOD FOR ESTIMATING MATRICES

The WAMS-based damping control design is comprised of two steps: estimating the matrices A and B in the current operating condition; designing the damping coefficients K_1 of VSCs based on the estimated A and B for a desired damping performance.

A. The Theoretical Basis of the WAMS-Based Method for Matrix Estimation

In the compact form of the power system dynamic model incorporating VSCs (14), $\boldsymbol{x}$ is a multivariate Ornstein-Uhlenbeck process. According to the regression theorem of a multivariate Ornstein-Uhlenbeck process [16], if the dynamic system described by (14) is stable which is typically satisfied if the system is in the normal operating condition, the τ-lag time correlation matrix $R(\tau)$ satisfies the following differential equation:

$$\frac{d}{d\tau}[R(\tau)] = A_c R(\tau) \tag{18}$$

where $R(\tau) \triangleq \left\langle [\boldsymbol{x}(t+\tau) - \bar{\boldsymbol{x}}], [\boldsymbol{x}(t) - \bar{\boldsymbol{x}}]^T \right\rangle$, and $\bar{\boldsymbol{x}}$ denotes the mean of $\boldsymbol{x}$. The τ-lag time correlation matrix describes the correlation of a random vector with itself at time lag τ. Therefore, the system state matrix can be obtained by solving (18) according to [17]

$$A_c = \frac{1}{\tau} \log \left[R(\tau) C^{-1} \right] \tag{19}$$

where the stationary covariance matrix $C \triangleq \left\langle [\boldsymbol{x}(t) - \bar{\boldsymbol{x}}], [\boldsymbol{x}(t) - \bar{\boldsymbol{x}}]^T \right\rangle = R(0)$.

Note that the statistics $R(\tau)$ and C of $\boldsymbol{x} = [\Delta\boldsymbol{\delta}, \Delta\boldsymbol{\omega}]^T$ can be estimated from PMU measurements (see Appendix B). Equation (19) indicates an ingenious way of estimating the physical model knowledge A_c from the statistical properties of PMU measurements, which serves as the theoretical basis of the proposed method for estimating matrices.

B. The Proposed Algorithm for Estimating Matrices

In order to estimate A and B in (15)-(16), we propose an algorithm to estimate the dynamic components $-M^{-1}D$, $\bar{A}_1$, and $\bar{A}_2$, respectively. We assume that all generator buses are equipped with PMUs so that generators' rotor angles and speeds in ambient conditions can be calculated using the approaches in [28], [29]. The equipment of PMUs at all generators might seem optimistic for now, yet is reasonable in the near future because of the wide adoption of PMUs worldwide [30]. In addition, we assume that VSCs are within their capability limits to provide damping and have enough controllability over the critical modes. Also, the current damping coefficients K_1 of VSCs in (17) are assumed to be known when the algorithm is initiated (i.e., the default setting or no support). The specific steps of the proposed algorithm are as follows:

Step 1: Given PMU measurements with a sufficient window length, estimate $[\Delta\boldsymbol{\delta}, \Delta\boldsymbol{\omega}]^T$ and compute their sample covariance matrix $\hat{C}$ and sample τ-lag correlation matrix $\hat{R}$ for a selected τ according to (32) and (33) in Appendix B. Estimate the closed-loop system state matrix by (19).

$$\hat{A}_{c1} = \left[\begin{array}{cc} 0 & \omega_0 I_{N_g} \\ A_{c1LL} & A_{c1LR} \end{array} \right] = \left[\begin{array}{cc} 0 & \omega_0 I_{N_g} \\ \bar{A}_1 & \bar{A}_2 K_1 - M^{-1}D \end{array} \right] \tag{20}$$

Step 2: Add small perturbations (e.g., $\alpha\%$) to the damping coefficients of all VSCs simultaneously by $K_1(i,j) \leftarrow K_1(i,j) + \Delta K_1(i,j)$, where $K_1 \in \mathbb{R}^{N_v \times N_g}$,

$$\Delta K_1(i,j) = \left\{ \begin{array}{ll} \alpha\% K_1(i,j), & j = g_i \\ 0, & j \neq g_i \end{array} \right. \tag{21}$$

where g_i represents the column of the entry that has the largest absolute value among $\{1, 2, ..., N_g\} \setminus \{g_1, ... g_{i-1}\}$ columns in the ith row of K_1.

More specifically, g_i is determined by the following steps. Starting from the first VSC (e.g., 1st row of K_1), let g_1 be the column number that has the largest absolute value in the 1st row; go to the 2nd VSC (i.e., 2nd row of K_1) and let g_2 be the column number that has the largest absolute value among $\{1, 2, ..., N_g\} \setminus \{g_1\}$ columns in the 2nd row. We continue the above procedure until the last row of K_1. As such, the perturbation matrix $\triangle K_1$ will be a generalized permutation matrix such that each column of $\bar{A}_2$ will be detectable in the estimation (see (24)).

Step 3: Collect new PMU measurements and estimate $[\Delta\boldsymbol{\delta}, \Delta\boldsymbol{\omega}]^T$ after the perturbation. Estimate the new system state matrix after the perturbation by (19):

$$\hat{A}_{c2} = \begin{bmatrix} 0 & \omega_0 I_{N_g} \\ A_{c2LL} & A_{c2LR} \end{bmatrix}$$
$$= \begin{bmatrix} 0 & \omega_0 I_{N_g} \\ \bar{A}_1 & \bar{A}_2(K_1 + \Delta K_1) - M^{-1}D \end{bmatrix} \quad (22)$$

Step 4: Estimate the dynamic components $\bar{A}_1$, $\bar{A}_2$ and $-M^{-1}D$ as follows:

$$\bar{A}_1^{est} = A_{c2LL} \quad (23)$$
$$\bar{A}_2^{est} = (A_{c2LR} - A_{c1LR})\Delta K_1^+ \quad (24)$$
$$(-M^{-1}D)^{est} = A_{c1LR} - \bar{A}_2^{est}K_1 \quad (25)$$

where ΔK_1^+ is the pseudo inverse matrix of ΔK_1.

Particularly, (24) is obtained by subtracting (20) from (22) using a simple manipulation to the lower-right part. Equation (25) is obtained by substituting $\bar{A}_2^{est}$ in (24) back to the lower-right part of (20).

Remarks:

- In this paper, a window size of 300s is used in **Step 1** and **Step 3**, respectively, for which a good accuracy is achieved. It should be noted that, despite of a relatively large window size, the above algorithm does not assume any model information (e.g. network topology, generator dynamic parameters D and M), but can estimate the dynamic components as well as the matrices A and B purely from PMU data. Therefore, in the case of incomplete or inaccurate network information, the proposed method provides a way to acquire the dynamical system model for monitoring or control if sufficient data is available.
- The way to choose g_i in **Step 2** is not unique. Different g_i can be selected as long as the resulting $\triangle K_1$ is a generalized permutation matrix such that each column of $\bar{A}_2$ is detectable in the estimation. Regarding the feasibility of adding perturbations to VSCs simultaneously, it can be realized by using the Global Positioning System (GPS) satellite and the high speed communication network between the control center and distributed VSCs. A more detailed implementation in the real systems can be found in [31], [32].
- The second-order generator model is assumed in the proposed algorithm. However, 3rd-order generator models with automatic voltage regulators (AVR) are used in the simulation study to show the effectiveness of the algorithm in practical applications.

IV. THE WAMS-BASED METHOD FOR WIDE-AREA DAMPING CONTROL

Once the dynamic components $-M^{-1}D$, $\bar{A}_1$ and $\bar{A}_2$ are estimated, A and B in (13) can be obtained from (15)-(16). Therefore, the control input $\boldsymbol{u}$ can be designed to provide effective damping. To this end, the MLQR [33] is applied

to design the system input $\boldsymbol{u}$ in (13) such that the following quadratic cost function is minimized:

$$J_C = \lim_{t\to\infty} E\left\{\int_0^t \left(\boldsymbol{x}^T(L^T W_Q L)\boldsymbol{x} + \boldsymbol{u}^T W_R \boldsymbol{u}\right)dt\right\} \quad (26)$$

where $W_Q \geq 0$ and $W_R > 0$ are weighting matrices which in most cases are set as diagonal matrices. In specific, higher diagonal values in W_Q correspond to a greater desire to stabilize the corresponding oscillation modes. Higher diagonal values in W_R represent a more strict requirement to reduce the corresponding control inputs. Note that only the relative sizes of the components in the weighting matrices matter rather than the absolute values. Besides, L is the mapping matrix obtained from the Real Schur Decomposition [34] of the system state matrix A, which transforms state variables $\boldsymbol{x}(t)$ to the modal variables $\boldsymbol{z}(t)$:

$$\boldsymbol{z}(t) = L\boldsymbol{x}(t) \quad (27)$$

where $\boldsymbol{z}$ are directly associated with system modes $e^{\lambda_i t}$, $i = 1, 2, ..., 2 \times N_g$. As a result, to damp the critical modes, we can add weights only to the corresponding diagonal values of W_Q while setting all the other values to be zero, making the well-damped modes unaffected by the control.

The MLQR controller gain Γ can be obtained by solving the associated algebraic Riccati equation (ARE) according to the cost function (26). The final MLQR feedback control law is:

$$\boldsymbol{u} = -\Gamma\boldsymbol{x} \quad (28)$$

The damping coefficients K_1 of VSCs, therefore, are set according to Γ.

The main advantage of the MLQR control method lies in the fact that a full decoupling between modes can be reached such that multiple critical modes can be damped simultaneously while well-damped modes remain unaffected, making the local controllers effective [33]. In addition, the VSCs' modulation capacities can be incorporated by tuning the weighting matrix W_R.

To sum up, the overall procedure for the online WAMS-based WADC method using VSCs is described in Fig. 2. It consists of two stages: the WAMS-based method for estimating matrices and the MLQR-based WADC design. The damping coefficients can be adjusted if the changes of working condition or network topology are detected. It should be noteworthy that if enough damping is provided by VSCs when the system works in the normal working condition, the system may still have suboptimal damping performance for the critical modes within the small time span after the event, when the controller is not updated yet. In the extreme case where very poor damping occurs, some emergency control strategy (e.g., PSS-based) using ring-down PMU data [35] can be incorporated.

V. CASE STUDIES

The IEEE 68-bus system is modified to test the proposed WAMS-based WADC method. In particular, three VSCs (denoted by VSC1, VSC2 and VSC3) are placed at bus 54, 20
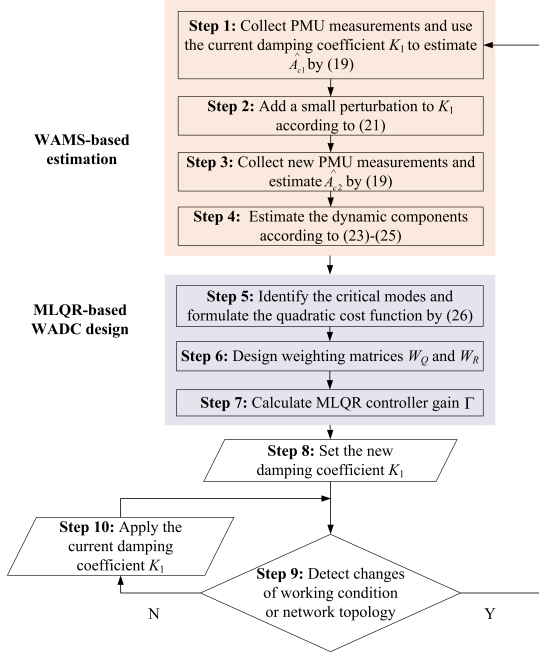
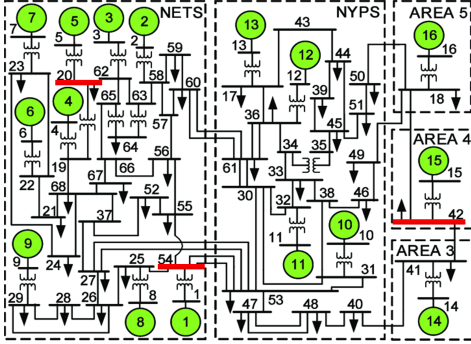Fig. 2. Flow chart of the WAMS-based WADC strategy.

Fig. 3. The network topology of the IEEE 68-bus system with integrated VSCs.

and 42 respectively, which are marked in red in Fig. 3. The implementation for different VSC locations will be discussed in Section V-E. In steady state, all VSCs inject the same amount of active power of 0.5 p.u. into the AC system and there are no reactive power exchanges. In order to validate the effectiveness of the proposed method in practical applications, the 3rd-order generator models are used throughout the simulations. In addition, G1-G12 are controlled by automatic voltage regulators (AVRs). The fluctuation intensities $\sigma_1, ..., \sigma_n$ describing load variations are all set to 0.05. $\tau = 100$ ms is used to calculate the correlation matrix (see (33)). All the simulations are done in the Power System Analysis Toolbox (PSAT) [36].

A. Validation For the Algorithm of Estimating Matrices

State variables $\boldsymbol{\delta}$ and $\boldsymbol{\omega}$ are obtained from the emulated PMU data with a sampling rate of 50 Hz and a window size of 300 s. For example, Fig. 4 presents the time-domain trajectory of G1's rotor speed before and after adding the small perturbation introduced in **Step 2** by (21). It can be
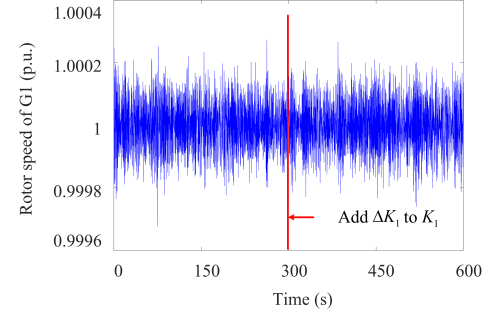

Fig. 4. Trajectories of G1's rotor speed before and after adding the small perturbation.

seen that the perturbation needed for estimating matrices is small and will not have an obvious impact on system performance. Following the procedure of the WAMS-based method of estimating matrices, the dynamic components are estimated and compared with their true values, as shown in Fig. 5. All matrices can be estimated with fairly good accuracy. Particularly, the entries with large values can always be well estimated, though some discrepancies may exist in the entries with smaller values, which, nevertheless, have little impact on the performance of the designed controllers as shown in the subsequent section. Besides, the impacts of PMU noise and missing PMUs on the matrix estimation using (19) have been discussed in [17], which shows that the closed-loop system state matrix A_c or its sub-matrix can still be well estimated. Readers are referred to [17] for more details. The subsequent discussions will focus on the effectiveness and the adpaptiveness of the proposed WAMS-Based WADC.
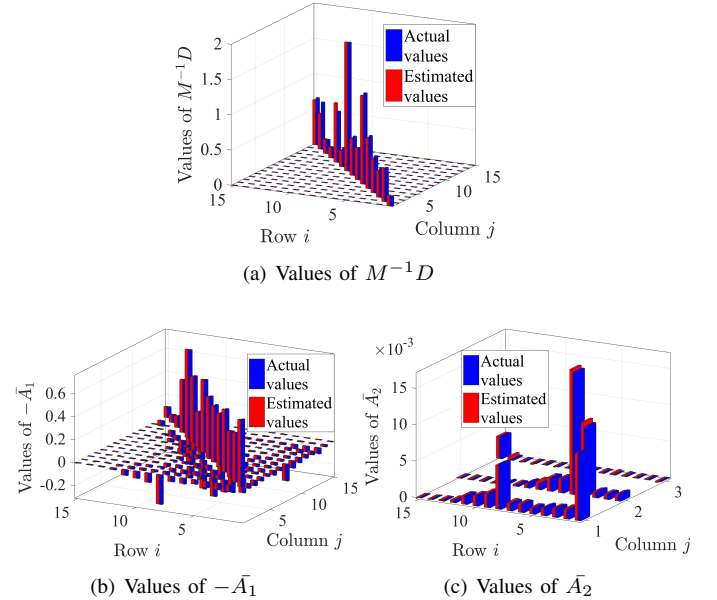

(a) Values of $M^{-1}D$

(b) Values of $-\bar{A}_1$

(c) Values of $\bar{A}_2$

Fig. 5. The actual and estimated values of the dynamic components.

B. Validation For the WAMS-Based WADC

The eigenvalues of the open-loop system state matrix are denoted in blue in Fig. 6(b), where all inter-area modes (those in the yellow circle) are poorly damped. In order to increase the damping ratios of the inter-area oscillations to 10%, above which the modes are considered to be well-damped [37], the WADC method introduced in section IV is applied. Specifically, the entries of the weighting matrix W_Q corresponding to three inter-area modes are adjusted until the design objective is achieved and the other entries are set to 0. In this case, the entries corresponding to three inter-area modes are set to 2, 2.7 and 65, respectively. Besides, an identity matrix is used for the weighting matrix W_R, which assumes that all VSCs have the same modulation capacities.

(a) Eigenvalues of the estimated system state matrix (b) Eigenvalues of the actual system state matrix
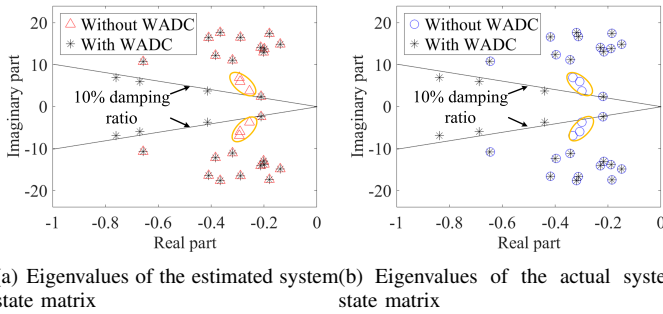
Fig. 6. Comparison of eigenvalues with and without WADC.

Fig. 6 presents the comparison of eigenvalues with and without applying the WADC method. The results based on the estimated matrices is shown in Fig. 6(a). It can be seen that the eigenvalues corresponding to the three critical inter-area modes all move to the left, making the damping ratios larger than 10%. Moreover, the WADC designed based on the estimation is still effective in the true system. As shown in Fig. 6(b), the damping ratios of all the critical inter-area modes of the true system have been increased above 10% by the designed WADC based on estimated matrices, indicating that multiple inter-area modes are damped simultaneously. In the mean time, the rest of modes are unaffected, demonstrating the decoupling between different modes by the proposed method. In addition, the proposed WADC method took only 0.25s on a regular laptop (Core i7-7500U @ 2.70GHz, 16 GB RAM) to estimate the matrices and to design MLQR, indicating negligible computational time and good feasibility in an online environment.

C. Dynamic response to system disturbances

To validate the effectiveness of the WAMS-based WADC method under different system disturbances, we test the performance of the proposed method in two situations—under the variation of load and generation and under a line fault.

1) Load and generation variation: In the first case, there is a sudden 10% generation decrease from G8-G10 and 10% load decrease from bus 17 at 50.0 s. The dynamic response of the rotor angle difference between G5 and G13 by applying the WAMS-based WADC method is compared to that with PSS

control, as shown in Fig. 7(a). It can be seen that the WAMS-based WADC method seems to be more effective than PSS in damping the inter-area oscillation modes. Fig. 7(b) presents the output active power of VSCs, showing the support of VSCs to damp the oscillations.
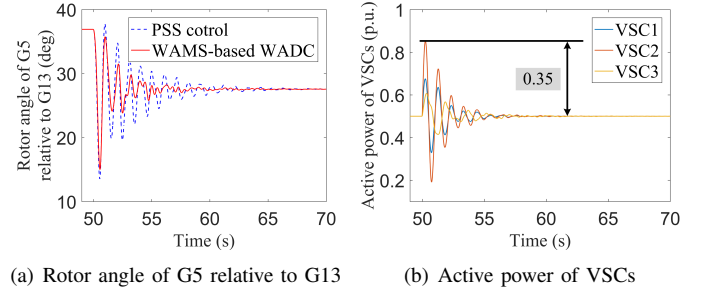

(a) Rotor angle of G5 relative to G13 (b) Active power of VSCs

Fig. 7. The system performance under a generation and load variation.

2) Line fault: In the second case, a three-phase line-to-ground fault is applied to bus 54 at 50.0 s and is cleared after 0.0833s. Similarly, the dynamic response of the relative angle between G5 and G13 is presented in Fig. 8(a). Obviously, a better damping performance is achieved using the proposed WAMS-based WADC method compared to the conventional PSS control. In addition, comparing the results in Fig. 8(b) with those in Fig. 7(b), we note that the maximum modulated power of VSC2 is increased from 0.35 p.u. to 0.51 p.u. when providing the damping support given that the line fault may be a more severe disturbance compared to the power variation of load and generation.

It should be noted that the communication delay in practical applications may deteriorate the damping performance, which, however, can be alleviated by appropriate compensation approaches (e.g., [38]).
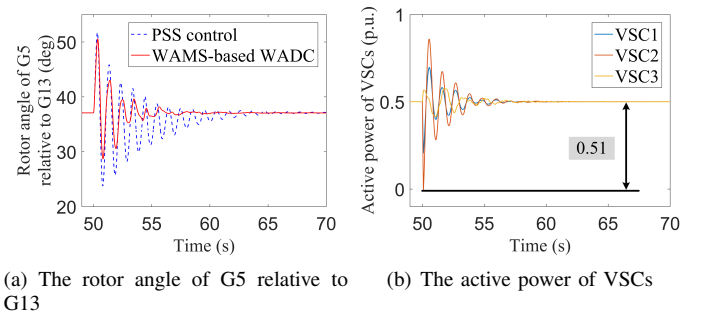

(a) The rotor angle of G5 relative to G13 (b) The active power of VSCs

Fig. 8. The system performance when there is a line-to-ground fault at bus 54.

D. Adaptiveness to different working conditions

In contrast to the model-based WADC, which may not consider the change of working conditions, a significant advantage of the proposed WAMS-based WADC method is that the damping coefficients can be adjusted as the working condition varies. To show this, the adaptiveness of the proposed method

TABLE I

An electromechanical mode (Mode 2) under different control strategies and working conditions when VSCs are located at buses 54, 20, 42

Working condition	Open-loop (without damping control)		Closed-loop (the model-based WADC)		Closed-loop (the WAMS-based WADC)	
	Frequency (Hz)	Damping ratio (%)	Frequency (Hz)	Damping ratio (%)	Frequency (Hz)	Damping ratio (%)
Base case	0.952	5.121	0.943	11.143	0.943	11.470
Line outage at bus 60-61	0.735	4.231	0.724	8.872	0.720	11.900
Line outage at bus 53-54	0.757	4.107	0.746	8.800	0.743	11.643
Generation and load variation followed by a line outage 53-54	0.727	3.780	0.717	7.989	0.715	11.209

to the individual line outage and a combined case where both line outage and load variations occur will be demonstrated. Specifically, three working conditions except the base case are considered: the condition after a line outage at bus 60-61; the condition after a line outage at bus 53-54; the condition after a sudden 10% load increase from bus 17 and 10% generation increase from G8-G10, followed by a line outage at bus 53-54 1s afterward.

The system performance without any control is compared to that with the model-based WADC using MLQR and that with the WAMS-based WADC using MLQR. We assume that the topology changes are undetected such that the model-based WADC designed for the base case remains unchanged. Table I presents the frequency and the damping ratio of an inter-area oscillation (Mode 2) under different control strategies and in various working conditions. It can be seen that both the model-based WADC and the WAMS-based WADC can increase the damping ratio to above 10% in the base case. However, Mode 2 changes from well-damped to poorly-damped when any of the aforementioned working conditions happens, whereas the model-based WADC fails to increase the damping ratio of Mode 2 to the requested 10%. The model-based WADC becomes ineffective when the working condition changes as the controller damping gain is not updated due to the undetected topology changes or load variations. In contrast, the WAMS-based WADC can always ensure that the minimum requested damping ratio is achieved when the working condition and/or the characteristics of electromechanical modes change. In addition, Fig. 9 shows comparisons of the time domain response when Mode 2 (0.952Hz) is excited in different working conditions with different control strategies. Obviously, we can see that the WAMS-based WADC can always achieve better damping performance than the model-based WADC. Note that the difference is not huge because the targeted damping ratio in the WAMS-based WADC is 10%. A higher damping ratio can be achieved by setting a higher threshold.

E. Validation for different VSCs' locations

In practice, VSCs may be located electrically far from the generations. As a result, the effectiveness of the proposed strategy by using VSCs at different locations is tested in this section. Generally speaking, the selection of the locations of VSCs can follow the controllability indexes. Interested readers can check more details in [39], [40]. The controllability analysis shows that VSCs added to bus 56 and 20 have a relative large controllability indexes associated with Mode 1
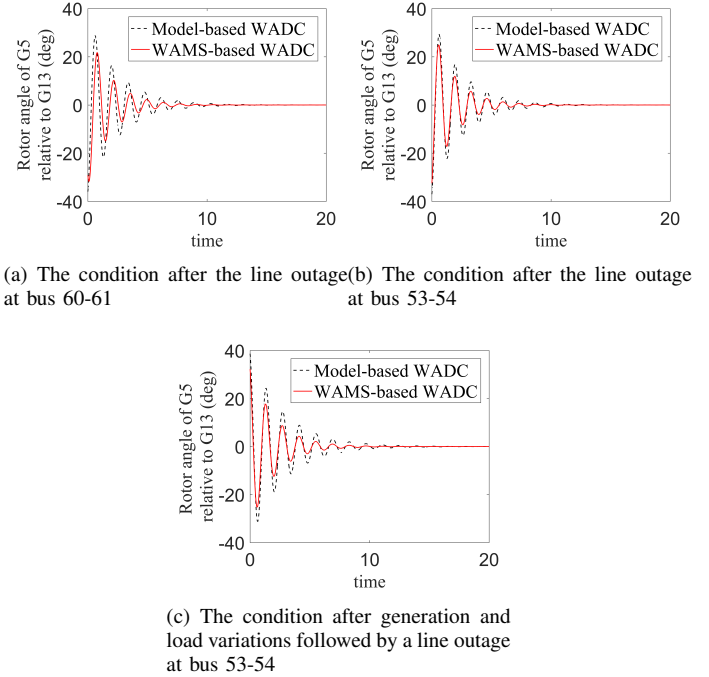

(a) The condition after the line outage at bus 60-61

(b) The condition after the line outage at bus 53-54

(c) The condition after generation and load variations followed by a line outage at bus 53-54

Fig. 9. The system response to Mode 2 in different working conditions with different control methods.

(a) Eigenvalues of the estimated system state matrix

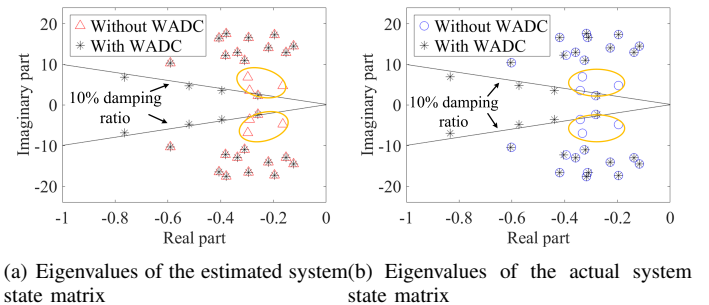(b) Eigenvalues of the actual system state matrix

Fig. 10. Comparison of eigenvalues with and without WADC when VSCs' locations change (at buses 56, 20, 42).

TABLE II

An electromechanical mode (Mode 2) under different control strategies and working conditions when VSCs are located at buses 56, 20, 42.

Working condition	Open-loop (without damping control)		Closed-loop (the model-based WADC)		Closed-loop (the WAMS-based WADC)	
	Frequency (Hz)	Damping ratio (%)	Frequency (Hz)	Damping ratio (%)	Frequency (Hz)	Damping ratio (%)
Base case	0.952	5.119	0.943	11.216	0.942	11.539
Line outage at bus 53-54	0.759	4.113	0.749	8.400	0.745	11.876
Generation and load variation followed by a line outage 53-54	0.729	3.796	0.720	7.656	0.714	12.412

(0.594Hz) and Mode 2 (0.952Hz). In comparison, the VSC added to bus 42 is more effective in Mode 1 and Mode 3 (1.108Hz). Therefore, a system with three VSCs placed at bus 56, 20 and 42 is considered, which has VSCs both far from and close to generators. More rigorous analysis on how to select the feedback signals and optimize the locations of VSCs for an effective control of multiple modes requires future effort.

Modal analysis shows that there are still three critical oscillation modes when damping control is not provided by VSCs. After applying the proposed WADC method, the damping ratios of the three modes can be successfully increased to above 10%, as presented in Fig. 10. Additionally, the adaptiveness of the WAMS-based WADC strategy is tested in three working conditions: the base working condition, the condition after a line outage at bus 53-54 as well as the condition after a generation and load variation followed by the line outage at bus 53-54, which is the same as the one applied in Section IV.D. The results summarized in Table. II validate that the proposed WAMS-based WADC control can always maintain the required damping ratio, which may not be achieved by the model-based WADC in different working conditions.

VI. Conclusion and Future Work

This paper has proposed a novel model-free WADC method to damp multiple inter-area oscillations using VSCs in various operation conditions. The method can be divided into two steps: the WAMS-based model-free estimation of the actual system state matrix A and the input matrix B, which is followed by the MLQR-based WADC method using the estimated matrices. The proposed method, being independent of model parameters and network topology, can adjust the control signals of VSCs to provide sufficient damping as the system evolves. Numerical studies in the modified IEEE 68-bus system show that the inter-area oscillations can always be well damped by the proposed method regardless of the change of working conditions and network topology. In the near future, robust control methods with respect to time delay will be studied. More detailed VSC dynamics and optimal placement of VSCs to provide damping will also be considered.

Appendix A

Firstly, the matrix of derivatives in (10) are expressed by

$$\begin{bmatrix} \frac{\partial \boldsymbol{P_E}}{\partial \boldsymbol{\delta}} & \frac{\partial \boldsymbol{P_E}}{\partial \boldsymbol{\theta}} & \frac{\partial \boldsymbol{P_E}}{\partial \boldsymbol{V}} \\ \frac{\partial \boldsymbol{P_v}}{\partial \boldsymbol{\delta}} & \frac{\partial \boldsymbol{P_v}}{\partial \boldsymbol{\theta}} & \frac{\partial \boldsymbol{P_v}}{\partial \boldsymbol{V}} \\ \frac{\partial \boldsymbol{Q_v}}{\partial \boldsymbol{\delta}} & \frac{\partial \boldsymbol{Q_v}}{\partial \boldsymbol{\theta}} & \frac{\partial \boldsymbol{Q_v}}{\partial \boldsymbol{V}} \end{bmatrix} = \begin{bmatrix} A_{11} & A_{12} & A_{13} \\ A_{21} & A_{22} & A_{23} \\ A_{31} & A_{32} & A_{33} \end{bmatrix} \quad (29)$$

Based on the second and third rows of (10), $\Delta\boldsymbol{\theta}$ and $\Delta\boldsymbol{V}$ can be calculated by

$$\begin{aligned} \Delta\boldsymbol{\theta} &= F_1 A_{23}{}^{-1} \left(\Delta\boldsymbol{P_v} - A_{21}\Delta\boldsymbol{\delta}\right) \\ &\quad - F_1 A_{33}{}^{-1} \left(\Delta\boldsymbol{Q_v} - A_{31}\Delta\boldsymbol{\delta}\right) \\ \Delta\boldsymbol{V} &= F_2 A_{22}{}^{-1} \left(\Delta\boldsymbol{P_v} - A_{21}\Delta\boldsymbol{\delta}\right) \\ &\quad - F_2 A_{32}{}^{-1} \left(\Delta\boldsymbol{Q_v} - A_{31}\Delta\boldsymbol{\delta}\right) \end{aligned} \quad (30)$$

where

$$\begin{aligned} F_1 &= \left(A_{23}{}^{-1} A_{22} - A_{33}{}^{-1} A_{32}\right)^{-1} \\ F_2 &= \left(A_{22}{}^{-1} A_{23} - A_{32}{}^{-1} A_{33}\right)^{-1} \end{aligned}$$

According to the first row of (10) and substituting $\Delta\boldsymbol{\theta}$ and $\Delta\boldsymbol{V}$ by (30), we have

$$\begin{aligned} \Delta\boldsymbol{P_E} &= A_{11}\Delta\boldsymbol{\delta} + A_{12}\Delta\boldsymbol{\theta} + A_{13}\Delta\boldsymbol{V} \\ &= A_1\Delta\boldsymbol{\delta} + A_2\Delta\boldsymbol{P_v} + A_3\Delta\boldsymbol{Q_v} \end{aligned} \quad (31)$$

where

$$\begin{aligned} A_1 &= A_{11} + A_{12}F_1 \left(-A_{23}{}^{-1} A_{21} + A_{33}{}^{-1} A_{31}\right) \\ &\quad + A_{13}F_2 \left(-A_{22}{}^{-1} A_{21} + A_{32}{}^{-1} A_{31}\right) \\ A_2 &= A_{12}F_1 A_{23}{}^{-1} + A_{13}F_2 A_{22}{}^{-1} \\ A_3 &= -A_{12}F_1 A_{33}{}^{-1} - A_{13}F_2 A_{32}{}^{-1} \end{aligned}$$

Appendix B

The estimated correlation matrix and the stationary covariance matrix are given by:

$$\begin{aligned} \hat{R}_{\boldsymbol{xx}}(\tau) &= \begin{bmatrix} \hat{R}_{\boldsymbol{\delta\delta}}(\tau) & \hat{R}_{\boldsymbol{\delta\omega}}(\tau) \\ \hat{R}_{\boldsymbol{\omega\delta}}(\tau) & \hat{R}_{\boldsymbol{\omega\omega}}(\tau) \end{bmatrix} \\ \hat{C}_{\boldsymbol{xx}} &= \begin{bmatrix} \hat{C}_{\boldsymbol{\delta\delta}} & \hat{C}_{\boldsymbol{\delta\omega}} \\ \hat{C}_{\boldsymbol{\omega\delta}} & \hat{C}_{\boldsymbol{\omega\omega}} \end{bmatrix} \end{aligned} \quad (32)$$

Each entry of $\hat{R}_{\boldsymbol{\delta\delta}}(\tau)$ and $\hat{C}_{\boldsymbol{\delta\delta}}$ can be computed by

$$\begin{aligned} \hat{R}_{\delta_i\delta_j}(\tau) &= \frac{1}{N}\sum_{k=1}^{N-\tau}\left(\delta_{(k+\tau)i} - \bar{\delta}_i\right)\left(\delta_{kj} - \bar{\delta}_j\right) \\ \hat{C}_{\delta_i\delta_j} &= \frac{1}{N}\sum_{k=1}^{N}\left(\delta_{ki} - \bar{\delta}_i\right)\left(\delta_{kj} - \bar{\delta}_j\right) \end{aligned} \quad (33)$$

where τ is a given lagging time, $\bar{\delta}_i$ is the mean value of δ_i, and N is the sample size. Likewise, $\hat{R}_{\boldsymbol{\delta\omega}}(\tau)$, $\hat{R}_{\boldsymbol{\omega\delta}}(\tau)$, $\hat{R}_{\boldsymbol{\omega\omega}}(\tau)$, $\hat{C}_{\boldsymbol{\delta\omega}}$, $\hat{C}_{\boldsymbol{\omega\delta}}$ and $\hat{C}_{\boldsymbol{\omega\omega}}$ can also be calculated.

References

[1] M. E. Aboul-Ela, A. Sallam, J. D. McCalley, and A. Fouad, "Damping controller design for power system oscillations using global signals," *IEEE Trans. Power Syst.*, vol. 11, no. 2, pp. 767–773, 1996.

[2] N. Mithulananthan, C. A. Canizares, J. Reeve, and G. J. Rogers, "Comparison of PSS, SVC, and STATCOM controllers for damping power system oscillations," *IEEE Trans. Power Syst.*, vol. 18, no. 2, pp. 786–792, 2003.

[3] R. Preece, J. V. Milanović, A. M. Almutairi, and O. Marjanovic, "Damping of inter-area oscillations in mixed AC/DC networks using wams based supplementary controller," *IEEE Trans. Power Syst.*, vol. 28, no. 2, pp. 1160–1169, 2012.

[4] J. Quintero, V. Vittal, G. T. Heydt, and H. Zhang, "The impact of increased penetration of converter control-based generators on power system modes of oscillation," *IEEE Trans. Power Syst.*, vol. 29, no. 5, pp. 2248–2256, 2014.

[5] L. Zhou, X. Yu, B. Li, C. Zheng, J. Liu, Q. Liu, and K. Guo, "Damping inter-area oscillations with large-scale PV plant by modified multiple-model adaptive control strategy," *IEEE Trans. Sustain. Energy*, vol. 8, no. 4, pp. 1629–1636, 2017.

[6] G. Tang, Z. Xu, H. Dong, and Q. Xu, "Sliding mode robust control based active-power modulation of multi-terminal HVDC transmissions," *IEEE Trans. Power Syst.*, vol. 31, no. 2, pp. 1614–1623, 2015.

[7] Y. Pipelzadeh, N. R. Chaudhuri, B. Chaudhuri, and T. C. Green, "Coordinated control of offshore wind farm and onshore HVDC converter for effective power oscillation damping," *IEEE Trans. Power Syst.*, vol. 32, no. 3, pp. 1860–1872, 2016.

[8] X. Fan, J. Shu, and B. Zhang, "Coordinated control of DC grid and offshore wind farms to improve rotor-angle stability," *IEEE Trans. Power Syst.*, vol. 33, no. 4, pp. 4625–4633, 2018.

[9] A. Yazdani and R. Iravani, *Voltage-sourced converters in power systems*. Wiley Online Library, 2010, vol. 34.

[10] M. Beza and M. Bongiorno, "An adaptive power oscillation damping controller by STATCOM with energy storage," *IEEE Trans. Power Syst.*, vol. 30, no. 1, pp. 484–493, 2014.

[11] N. T. Trinh, I. Erlich, and S. P. Teeuwsen, "Methods for utilization of MMC-VSC-HVDC for power oscillation damping," in *Proc. IEEE PES General Meeting*, Jul. 2014, pp. 1–5.

[12] Y. Li, C. Rehtanz, S. Ruberg, L. Luo, and Y. Cao, "Wide-area robust coordination approach of HVDC and FACTS controllers for damping multiple interarea oscillations," *IEEE Trans. Power Del.*, vol. 27, no. 3, pp. 1096–1105, 2012.

[13] I. Zenelis and X. Wang, "Wide-area damping control for interarea oscillations in power grids based on PMU measurements," *IEEE Contr. Syst. Lett.*, vol. 2, no. 4, pp. 719–724, 2018.

[14] V. Pradhan, A. Kulkarni, and S. Khaparde, "A model-free approach for emergency damping control using wide area measurements," *IEEE Trans. Power Syst.*, vol. 33, no. 5, pp. 4902–4912, 2018.

[15] X. Zhang, C. Lu, S. Liu, and X. Wang, "A review on wide-area damping control to restrain inter-area low frequency oscillation for large-scale power systems with increasing renewable generation," *Renew. Sustain. Energy Rev.*, vol. 57, pp. 45–58, 2016.

[16] C. Gardiner, *Stochastic Methods: A Handbook for the Natural and Social Sciences*. Springer Berlin, 2009, vol. 4.

[17] H. Sheng and X. Wang, "Online measurement-based estimation of dynamic system state matrix in ambient conditions," *IEEE Trans. Smart Grid*, 2019, doi: 10.1109/TSG.2019.2917672.

[18] R. Singh, B. C. Pal, and R. A. Jabr, "Statistical representation of distribution system loads using gaussian mixture model," *IEEE Trans. Power Syst.*, vol. 25, no. 1, pp. 29–37, 2009.

[19] T. Odun-Ayo and M. L. Crow, "An analysis of power system transient stability using stochastic energy functions," *Int. Trans. Elect. Energy Syst.*, vol. 23, no. 2, pp. 151–165, 2013.

[20] X. Wang, J. W. Bialek, and K. Turitsyn, "PMU-based estimation of dynamic state jacobian matrix and dynamic system state matrix in ambient conditions," *IEEE Trans. Power Syst.*, vol. 33, no. 1, pp. 681–690, 2017.

[21] R. Preece, J. V. Milanovic, A. M. Almutairi, and O. Marjanovic, "Probabilistic evaluation of damping controller in networks with multiple VSC-HVDC lines," *IEEE Trans. Power Syst.*, vol. 28, no. 1, pp. 367–376, 2012.

[22] M. Mokhtari and F. Aminifar, "Toward wide-area oscillation control through doubly-fed induction generator wind farms," *IEEE Trans. Power Syst.*, vol. 29, no. 6, pp. 2985–2992, 2014.

[23] M. Singh, A. J. Allen, E. Muljadi, V. Gevorgian, Y. Zhang, and S. Santoso, "Interarea oscillation damping controls for wind power plants," *IEEE Trans. Sustain. Energy*, vol. 6, no. 3, pp. 967–975, 2014.

[24] A. S. Brouwer, M. Van Den Broek, A. Seebregts, and A. Faaij, "Impacts of large-scale intermittent renewable energy sources on electricity systems, and how these can be modeled," *Renew. Sustain. Energy Rev.*, vol. 33, pp. 443–466, 2014.

[25] J. Machowski, Z. Lubosny, J. W. Bialek, and J. R. Bumby, *Power system dynamics: stability and control*. John Wiley & Sons, 2020.

[26] P. M. Anderson and A. A. Fouad, *Power system control and stability*. John Wiley & Sons, 2008.

[27] Y. Wang, L. Da Silva, W. Xu, and Y. Zhang, "Analysis of ill-conditioned power-flow problems using voltage stability methodology," *IEE Proc.-Gener., Transmiss. Distrib.*, vol. 148, no. 5, pp. 384–390, 2001.

[28] N. Zhou, D. Meng, Z. Huang, and G. Welch, "Dynamic state estimation of a synchronous machine using PMU data: A comparative study," *IEEE Trans. Smart Grid*, vol. 6, no. 1, pp. 450–460, 2014.

[29] J. Yan, C.-C. Liu, and U. Vaidya, "PMU-based monitoring of rotor angle dynamics," *IEEE Trans. Power Syst.*, vol. 26, no. 4, pp. 2125–2133, 2011.

[30] Y. C. Chen, J. Wang, A. D. Domínguez-García, and P. W. Sauer, "Measurement-based estimation of the power flow Jacobian matrix," *IEEE Trans. Smart Grid*, vol. 7, no. 5, pp. 2507–2515, 2015.

[31] C. W. Taylor, D. C. Erickson, K. E. Martin, R. E. Wilson, and V. Venkatasubramanian, "WACS-wide-area stability and voltage control system: R&D and online demonstration," *Proc. IEEE*, vol. 93, no. 5, pp. 892–906, 2005.

[32] L. Peng, W. Xiaochen, L. Chao, S. Jinghai, H. Jiong, H. Jingbo, Z. Yong, and X. Aidong, "Implementation of CSG's wide-area damping control system: Overview and experience," in *Proc. IEEE/PES, Power Syst. Conf. Expo.*, 2009, pp. 1–9.

[33] A. Almutairi and J. Milanovic, *Enhancement of power system stability using wide area measurement system based damping controller*. University of Manchester, 2010.

[34] G. H. Golub and C. F. V. Loan, *Matrix Computations, 4th edition*. Johns Hopkins University Press, 2012.

[35] V. Pradhan, A. Kulkarni, and S. Khaparde, "A model-free approach for emergency damping control using wide area measurements," *IEEE Trans. Power Syst.*, vol. 33, no. 5, pp. 4902–4912, 2018.

[36] F. Milano, "An open source power system analysis toolbox," *IEEE Trans. Power Syst.*, vol. 20, no. 3, pp. 1199–1206, 2005.

[37] G. Rogers, *Power system oscillations*. Springer Science & Business Media, 2012.

[38] N. R. Chaudhuri, S. Ray, R. Majumder, and B. Chaudhuri, "A new approach to continuous latency compensation with adaptive phasor power oscillation damping controller (POD)," *IEEE Trans. Power Syst.*, vol. 25, no. 2, pp. 939–946, 2009.

[39] H. Latorre and M. Ghandhari, "Improvement of power system stability by using a VSC-HVDC," *Int. J. Electr. Power Energy Syst.*, vol. 33, no. 2, pp. 332–339, 2011.

[40] N. T. Trinh and I. Erlich, "Analytical investigation of factors influencing controllability of MMC-VSC-HVDC on inter-area and local oscillations in interconnected power systems," in *Proc. IEEE PES General Meeting*. Boston, MA, USA, 2016, pp. 1–5.

Jinpeng Guo (S'19) received the B.S. degree in electrical engineering and automation from Chongqing University, Chongqing, China, in 2014 and M.S. degree in electrical engineering from Southeast University, Nanjing, China, in 2017. He is currently pursuing the Ph.D. degree in the Department of Electrical and Computer Engineering, McGill University, Montreal, QC, Canada. His research interests include power system monitoring, analysis and control.
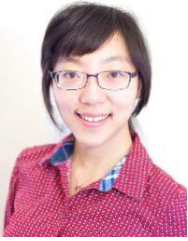
Xiaozhe Wang (S'13-M'16) is currently an Assistant Professor in the Department of Electrical and Computer Engineering at McGill University, Montreal, QC, Canada. She received the Ph.D. degree in the School of Electrical and Computer Engineering from Cornell University, Ithaca, NY, USA, in 2015, and the B.S. degree in Information Science and Electronic Engineering from Zhejiang University, Zhejiang, China, in 2010.

Her research interests are in the general areas of power system stability and control, uncertainty quantification in power system security and stability, and wide-area measurement system (WAMS)-based detection, estimation, and control. She is serving on the editorial boards of IEEE Transactions on Power Systems, Power Engineering Letters, and IET Generation, Transmission and Distribution.
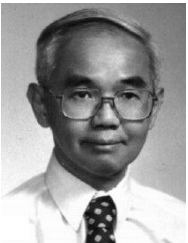
Boon-Teck Ooi (M'71-SM'85-F'02-LF'05) was born in Malaysia. He received the B. Eng. (Honors) degree in electrical engineering from the University of Adelaide, Australia, the M.S. degree in electrical engineering from the Massachusetts Institute of Technology and the Ph.D. degree in electrical engineering from McGill University, Montreal, QC, Canada. He is Emeritus Professor with the Department of Electrical and Computer Engineering, McGill University. He is IEEE Life Fellow.

His research interests are in linear and conventional electric motors and generators (steady-state, transient, stability); power electronics (voltage-source converters, current-source converters, multi-level converters, power quality, thyristor HVDC, PWM-HVDC, multi-terminal HVDC FACTS), wind and other renewable energy sources.